

Elena Witt*, Suliman Nakhal, C. Vinod Chandran, Martin Lerch, and Paul Heitjans

NMR and Impedance Spectroscopy Studies on Lithium Ion Diffusion in Microcrystalline γ -LiAlO₂

DOI 10.1515/zpch-2015-0587

Received February 27, 2015; accepted August 5, 2015

Abstract: In this work nuclear magnetic resonance (NMR) and impedance spectroscopy (IS) studies on Li ion dynamics in microcrystalline γ -LiAlO₂ are presented. The sample was prepared by solid state synthesis between Li₂CO₃ and Al₂O₃ in air, followed by a quenching procedure. The presence of phase-pure γ -LiAlO₂ was confirmed by X-ray powder diffraction including Rietveld refinement. Further structural characterization was done with ⁶Li, ⁷Li and ²⁷Al NMR. Several NMR techniques such as spin-lattice relaxation measurements, motional narrowing experiments, as well as spin-alignment echo were employed for the investigation of Li ion diffusion. The measurements were carried out at high temperatures (up to 970 K) in order to access the regime of Li ion motion being very slow. The dc conductivities measured by IS in the temperature range from 680 K to 870 K were converted to diffusion coefficients being compatible with those obtained by NMR.

Keywords: LiAlO₂, Lithium Ion Diffusion, Nuclear Magnetic Resonance, Impedance Spectroscopy

Dedicated to Professor Hans Ackermann on the occasion of his 80th birthday

*Corresponding author: Elena Witt, Institut für Physikalische Chemie und Elektrochemie, and ZFM – Center for Solid State Chemistry and New Materials, Leibniz Universität Hannover, Callinstr. 3–3a, 30167 Hannover, Germany, e-mail: witt@pci.uni-hannover.de

C. Vinod Chandran, Paul Heitjans: Institut für Physikalische Chemie und Elektrochemie, and ZFM – Center for Solid State Chemistry and New Materials, Leibniz Universität Hannover, Callinstr. 3–3a, 30167 Hannover, Germany

Suliman Nakhal, Martin Lerch: Institut für Chemie, Technische Universität Berlin, Straße des 17. Juni 135, 10623 Berlin, Germany

1 Introduction

Lithium compounds have been intensively studied during the last few decades (see, e.g., [1–6]). The main reason for this large interest is the attractive application possibility of these materials as ion conductors in the field of energy storage. Fast ionic motion is preferred in battery electrolytes [7] whereas the electrolyte additives are designed to have extremely slow ionic diffusion [8–10] for stability reasons. Small Li diffusivity is important also for some industrial applications such as in semiconductor manufacture [11] and in fusion reactors [12]. But the proper understanding of slow diffusion phenomena is very challenging. Therefore, fundamental research to elucidate the physical background of the slow dynamics is highly significant.

γ -LiAlO₂, being a poorly conducting material with a diffusion coefficient of about 10^{-26} m²/s at 298 K [13], serves as a good coating of Li electrodes [14]. In addition, it finds application as a tritium breeding material in fusion reactors [15] and as a substrate for the epitactic growth of III-V semiconductors [11], mainly because of its slow ionic diffusion properties.

In the present work, ultra-slow Li ionic motion in microcrystalline γ -LiAlO₂ has been investigated using nuclear magnetic resonance (NMR) and impedance spectroscopy (IS). With the help of solid-state NMR, the microscopic aspects of ionic diffusion are probed, while the macroscopic diffusion parameters are obtained from IS. Apart from studies with other methods [16–18], there are only a few publications about Li motions in this material investigated by NMR. Indris et al. studied γ -LiAlO₂ single crystals grown by the Czochralski technique [13, 19]. Wohlmuth et al. investigated nanocrystalline γ -LiAlO₂, prepared by ball milling [20]. We have studied the diffusivities of microcrystalline γ -LiAlO₂, synthesized by solid-state route.

2 Experimental

2.1 Solid state synthesis

For the synthesis of γ -LiAlO₂, lithium carbonate Li₂CO₃ (Aldrich, 99.997%) and α -aluminium oxide Al₂O₃ (Alfa Aesar, 99.98%) were used as starting materials in an appropriate molar ratio (1 : 1). The carefully mixed powders were pressed to pellets and slowly heated up to 1373 K. After 20 h at 1373 K, the pellets were quenched by removing them quickly out of the furnace. The powder was chemi-

cally characterized using a LECO EF-TC 300 N₂/O₂ analyzer (hot gas extraction) for oxygen content determination.

2.2 X-ray diffraction

For powder X-ray diffraction, we used a “PANalyticalX’Pert PRO MPD” diffractometer in Bragg-Brentano ($\theta-\theta$) geometry equipped with a Cu- $K\alpha$ source and a “PIXcel” detector. Rietveld refinements were carried out with the FULLPROF 2006 program package using pseudo-Voigt profile functions [21].

2.3 Nuclear magnetic resonance

For the NMR measurements two spectrometers were used: a Bruker MSL 100 (connected to a field-variable Oxford cryomagnet) at a frequency of 38.8 MHz for ⁷Li resonance and a Bruker Avance III 600 with 233.3 MHz as ⁷Li resonance frequency.

Structural investigations (⁶Li, ⁷Li and ²⁷Al NMR) were carried out using the Avance III 600 spectrometer. A 2.5 mm probe was used for magic-angle spinning (MAS) experiments at 10 kHz rotation frequency. The spectra were referenced to dilute solutions of lithium chloride and aluminium nitrate.

Temperature-dependent static ⁷Li NMR line shapes were recorded with the MSL 100 spectrometer. A home-built probe was used in order to carry out high-temperature NMR experiments (298 K–873 K).

Spin-lattice relaxation (SLR) rates were measured with the Avance III 600 spectrometer. The sample was rotated at 3 kHz. For measuring SLR rates in the laboratory frame of reference the saturation recovery pulse sequence was used ($10 \times (\pi/2) - t_{\text{delay}} - \pi/2 - \text{acquisition}$). The magnetization transients were fitted with a stretched exponential function. SLR rate measurements in the rotating frame of reference were performed using a spin-lock frequency of 23 kHz. High-temperature measurements (up to 973 K) were carried out with a laser-heated 7 mm MAS probe.

The decay of ⁷Li spin-alignment echoes (SAE) was monitored with the MSL 100 spectrometer under static conditions. For this, the Jeener-Broekaert pulse sequence [22] was used:

$$(\pi/2)_X - t_p - (\pi/4)_Y - t_m - (\pi/4)_\delta - \text{acquisition}.$$

While the preparation time (t_p) of 10 μ s was kept constant, the mixing time (t_m) was varied between 100 μ s and 100 s.

2.4 Impedance spectroscopy

Impedance measurements were carried out under argon atmosphere using a HP 4192 analyzer with a home-built cell in the temperature range between 298 and 900 K and in the frequency range from 5 Hz to 13 MHz. A Eurotherm controller was used to monitor and adjust the temperature. The powder was pressed to a pellet with 8 mm diameter and 1 mm thickness applying a pressure of 0.4 GPa at room temperature. On the pellet a Pt layer was deposited by sputtering. The sample was held at each temperature for 30 min before measuring.

3 Results and discussion

3.1 Structure characterization

After synthesis, the microcrystalline γ -LiAlO₂ sample was characterized by XRD. In Figure 1, the XRD patterns are shown together with the results from Rietveld refinement analysis. The phase purity of the material is clearly confirmed. In Figure 2, the crystal structure of γ -LiAlO₂ is shown. It crystallizes in the tetragonal space group P4₁2₁2 with a density of 2.62 g/cm³ [23]. The lattice consists of AlO₄ and LiO₄ tetrahedra connected with each other [24].

Further γ -LiAlO₂ structure investigations were performed by NMR spectroscopy. In particular, ²⁷Al MAS NMR was used for the determination of the environment of Al. For ²⁷Al (spin $I = 5/2$) the central transition signal is broadened because of quadrupolar interactions. Thus, the static ²⁷Al spectra cannot be used to obtain high resolution information for the structural characterization. To average these interactions magic-angle spinning (MAS) NMR was applied [25]. Figure 3a shows the ²⁷Al MAS NMR spectrum of γ -LiAlO₂ with the central transition positioned at 80 ppm. This chemical shift corresponds to tetrahedrally coordinated Al-O [24]. The two small signals marked by asterisks are side bands caused by spinning.

Furthermore, ⁶Li and ⁷Li NMR spectra of γ -LiAlO₂ were recorded. Since the ⁶Li nucleus (spin $I = 1$) has a much smaller quadrupole moment ($Q = -0.08 \text{ fm}^2$ [26]) than ⁷Li ($I = 3/2$, $Q = -4.1 \text{ fm}^2$ [27]), the ⁶Li MAS NMR spectrum provides higher resolution than that of ⁷Li. So, ⁶Li NMR can give more accurate information about the number of different Li sites in the crystal. The ⁶Li spectrum of γ -LiAlO₂ shows only one NMR signal (Figure 3b), confirming the presence of a single Li site in our γ -LiAlO₂ sample. The ⁷Li static NMR spectrum clearly shows a quadrupolar contribution (Figure 3c). The quadrupolar coupling con-

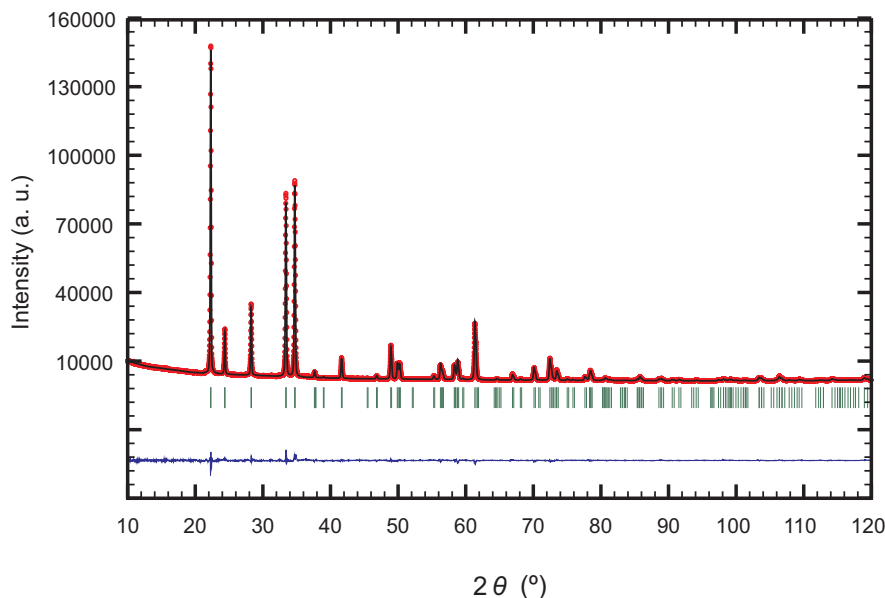


Figure 1: X-ray powder diffractogram of γ -LiAlO₂ with the results of Rietveld refinement.

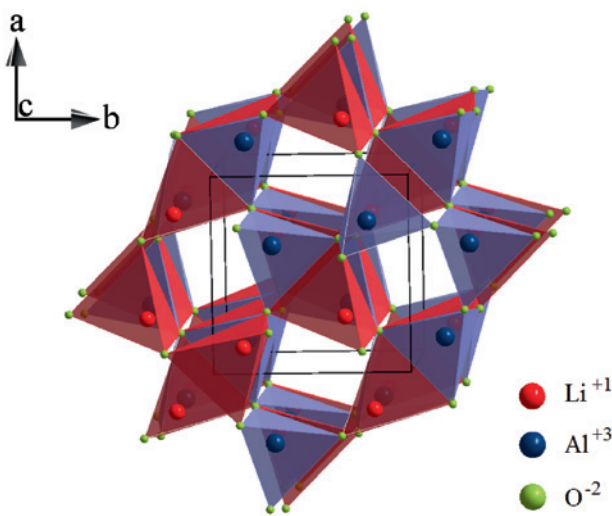


Figure 2: The crystal structure of γ -LiAlO₂ (tetragonal unit cell in black).

stant C_Q can be calculated from the line shape of the ^{7}Li NMR signal which was recorded using the solid echo pulse sequence [25]. The largest quadrupolar splitting, simulated by DMFIT [28], yields a quadrupolar coupling constant of about 95 kHz. It is consistent with C_Q of single crystalline γ -LiAlO₂ [19].

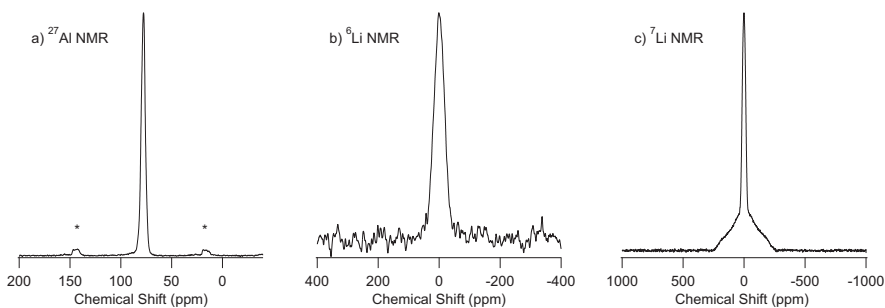


Figure 3: Structure characterization of microcrystalline γ - LiAlO_2 : ^{27}Al MAS (a), ^6Li (b) and ^7Li (c) static solid-echo NMR spectra at room temperature. The rotation frequency in the case of ^{27}Al MAS was 10 kHz.

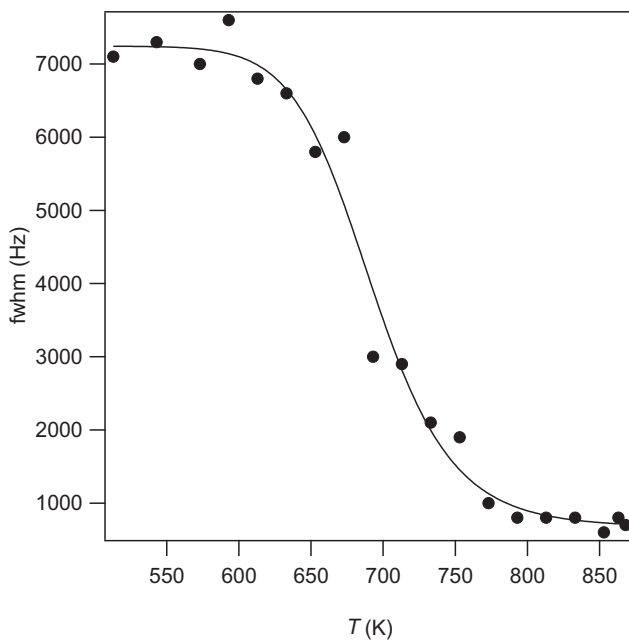


Figure 4: Motional narrowing: ^7Li NMR line width (full width at half-maximum) plotted against temperature. The line is to guide the eye.

3.2 Dynamics investigations

To probe Li ion diffusion, the temperature dependence of the ^7Li NMR line width was investigated under static conditions. At low temperatures broad lines were observed. On heating the Li ion motion gets faster, which eventually averages the

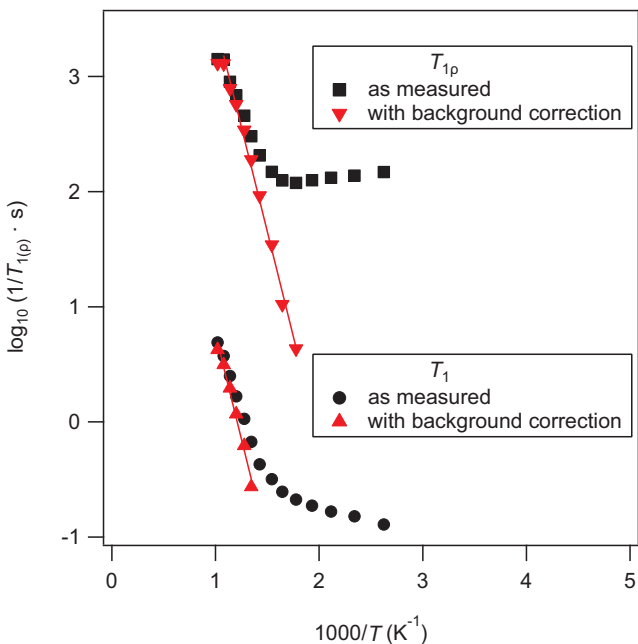


Figure 5: ^7Li NMR relaxation measurements: relaxation rate ($1/T_1$ and $1/T_{1p}$, respectively) dependence on inverse temperature in the laboratory (233 MHz) and rotating (23 kHz) frames of reference.

Li-Li dipolar couplings. Consequently the NMR line width decreases. This motional narrowing effect is often used to get first insights into the jump processes in solids [2]. In Figure 4 the full width at half-maximum (fwhm) plotted against temperature is shown. For the microcrystalline γ -LiAlO₂, the motional narrowing starts at 600 K. For γ -LiAlO₂ single crystals a similar result was presented by Indris et al. [13]. In the case of nanocrystalline γ -LiAlO₂, the motional narrowing starts at a lower temperature due to the comparably faster diffusion in such structures [4, 20].

NMR SLR measurements are widely used for studying Li ion diffusion [2]. Temperature dependent SLR times in the laboratory (T_1) and rotating (T_{1p}) frames of references are monitored. The semi-logarithmic plot of the SLR rates against inverse temperature shows a diffusion-induced maximum. The mean ionic jump rates can be estimated from the maximum of the rate peak. The shape of the peak indicates the activation energy for ionic jumps, the dimensionality of the diffusion pathway, and correlation effects [29]. In the present work, the SLR times T_1 of γ -LiAlO₂ were measured at a ^7Li Larmor frequency of 233 MHz. At room temperature T_1 was about 7 s. The influence of diffusion on the measured SLR rate T_1^{-1}

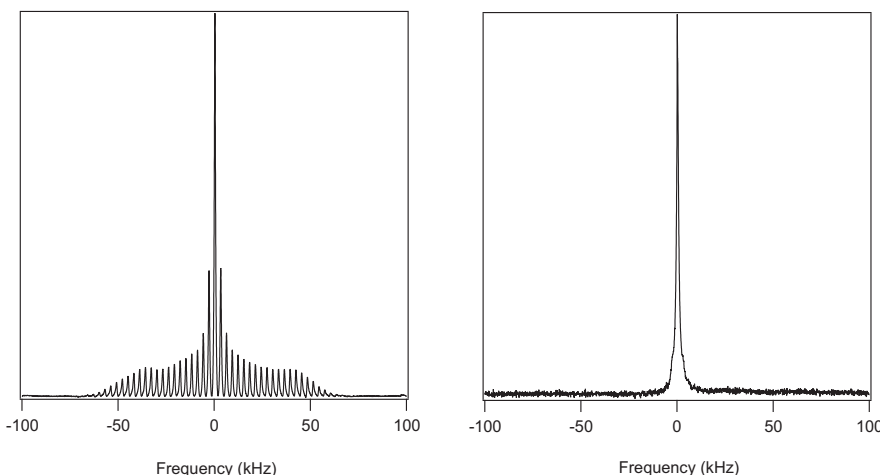


Figure 6: Averaging of quadrupolar interactions: ${}^7\text{Li}$ MAS NMR spectra at 298 K (on the left) and at 973 K (on the right) recorded at a resonance frequency of 233 MHz and with a rotation frequency of 3 kHz.

was detectable in the temperature regime from about 473 K to 973 K (Figure 5). Since the diffusion in $\gamma\text{-LiAlO}_2$ is very slow, only the low-temperature flank of the diffusion-induced rate peak could be observed at the above-mentioned conditions. Nevertheless, the low-temperature flank, which is sensitive to local Li^+ hopping, can be analyzed to determine the apparent activation energy of this diffusion process. After a correction of the measured SLR rates with respect to non-diffusive contributions extrapolated from the data at lower temperatures (“SLR background”, see, e.g., [8]), an Arrhenius fit of this flank gives an activation energy of about 0.7 eV.

In addition, relaxation times in the rotating frame of reference ($T_{1\rho}$) were measured (Figure 5). This technique allows a reduction of the effective field frequency to the order of kHz. As a consequence, the diffusion-induced rate peak shifts to lower temperatures. For the $T_{1\rho}$ measurements, a spin-lock field with a frequency of $\omega_1/2\pi = 23$ kHz was applied. The analysis of the $T_{1\rho}^{-1}$ low-temperature flank yields an activation energy of about 0.7 eV. This is in agreement with the value calculated from the T_1^{-1} flank. Only the very beginning of the high-temperature flank of $T_{1\rho}^{-1}$ could be observed (Figure 5). Assuming that the two identical $T_{1\rho}^{-1}$ values define the maximum of the rate peak, we can estimate the jump rate (τ^{-1}) at 973 K using the maximum condition for $T_{1\rho}^{-1}$ peak ($\tau \times \omega_1 \approx 0.5$). Therefore, from the $T_{1\rho}^{-1}$ peak, the Li ionic jump rate can be estimated as $2.9 \times 10^5 \text{ s}^{-1}$. This

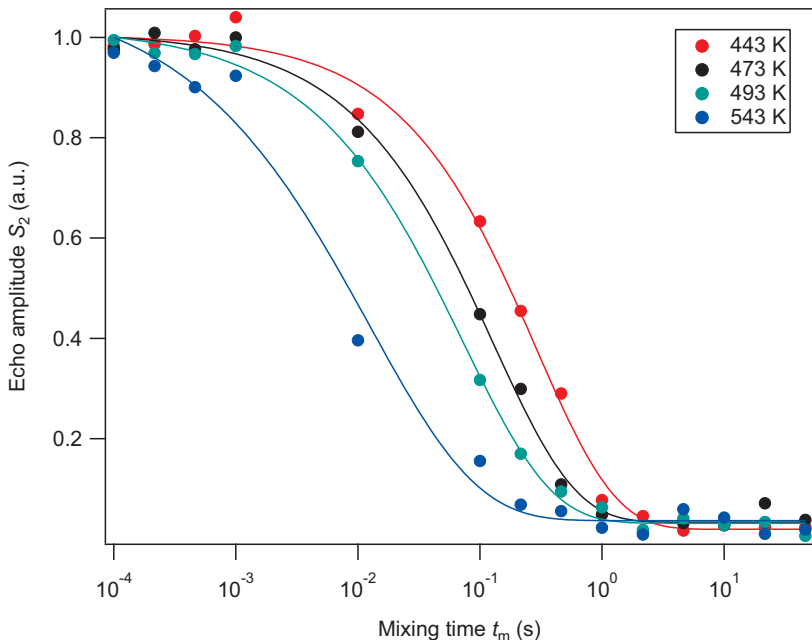


Figure 7: ${}^7\text{Li}$ spin-alignment echo NMR measurements: the echo amplitudes S_2 as a function of mixing times (t_m) at different temperatures.

result is in very good agreement with the jump rate deduced from the motional averaging of the ${}^7\text{Li}$ quadrupole interaction at high temperatures (cf. Figure 6). At low temperatures, the ${}^7\text{Li}$ MAS NMR signal shows spinning side bands due to partial averaging of the quadrupole coupling. But at 973 K, these quadrupole side bands vanish, indicating a complete averaging of the quadrupole interaction (Q_{avg}) due to the fast Li motion (cf., e.g., [30]). Since the C_Q of microcrystalline γ -LiAlO₂ is 95 kHz, a Li jump rate of 10^5 s^{-1} can be estimated.

To probe Li ion diffusion at a different time scale, spin-alignment echo (SAE) NMR was applied. This technique has been proved to be advantageous to study extremely slow motions at relatively low temperatures [8]. Contrary to NMR relaxometry, SAE NMR provides direct access to jump rates. The mixing time (t_m) dependent decay of the spin-alignment echo amplitude is shown in Figure 7. The temperature regime where the echo decay was influenced by diffusion was between 443 K and 543 K. The jump rates τ^{-1} calculated are in the range from 6 to 600 s^{-1} . They obey the Arrhenius law

$$\tau^{-1} = \tau_0^{-1} e^{-E_a/k_B T} \quad (1)$$

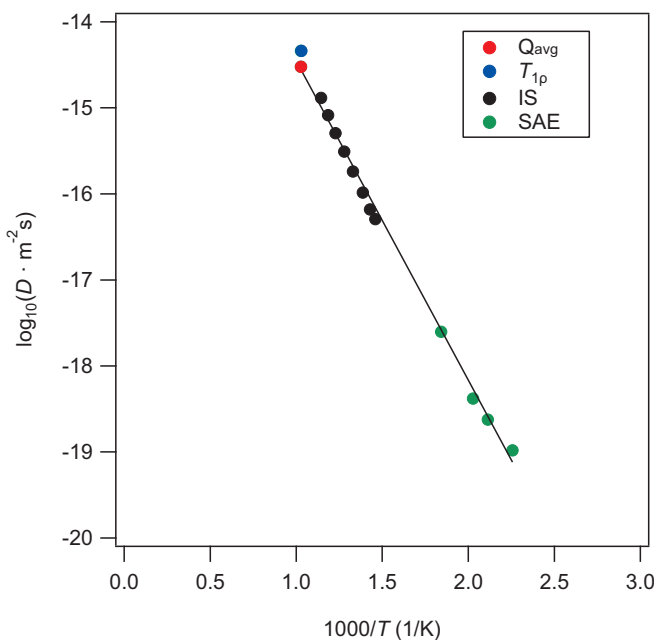


Figure 8: Comparison of γ -LiAlO₂ diffusivities derived from different methods: The solid line is the Arrhenius fit for the results from ⁷Li SAE and solid echo NMR (Q_{avg}) yielding an activation energy of 0.7 eV.

and give an activation energy E_a of about 0.7 eV, similar to that derived from the relaxation measurements. Here, τ_0^{-1} is the pre-exponential factor, k_B the Boltzmann constant, and T the temperature.

If we assume 3D diffusion and uncorrelated jumps of Li in LiAlO₂ the diffusion coefficient D can be calculated from the average jump rate τ^{-1} using the Einstein-Smoluchowski equation

$$D = l^2/6\tau \quad (2)$$

where l is the jump distance. Here, the shortest Li-Li distance (3.091 Å [13]) in γ -LiAlO₂ was taken. The results are plotted in Figure 8.

For a macroscopic point of view of diffusion in γ -LiAlO₂, impedance spectroscopy was applied. The spectra of the real part of the conductivity versus frequency as isotherms were recorded. The conductivities σ_{dc} were derived from frequency-independent plateaus of isotherms showing up in the low-frequency regime. From σ_{dc} diffusion coefficients were calculated by the Nernst-Einstein equation

$$D = T\sigma_{dc}k_B/(Nq^2) \quad (3)$$

where N is the number density of mobile Li ions ($2.39 \times 10^{28} \text{ m}^{-3}$ for γ -LiAlO₂ [13]), and q is their charge.

These also follow the Arrhenius law

$$D = D_0 e^{-E_a/k_B T} \quad (4)$$

The activation energy was found to be 0.9 eV for the temperature range between 680 K and 870 K (Figure 8). Secondary ion mass spectrometry (SIMS) showed a similar activation energy of 0.9 eV for amorphous LiAlO₂ [31]. As expected, the values of diffusion coefficients occurred to be higher in the amorphous material than in the microcrystalline form despite the similar activation energies. This indicates that the pre-exponential factor D_0 (Eq. 3) is higher for the amorphous material which has quite often been found (see, e.g., [32–34]). The Li diffusivities of the nanocrystalline γ -LiAlO₂ samples reported in the literature [20] are also higher than those presented here for the microcrystalline form, and the activation energy varies from 0.78 to 1.14 eV depending on the milling time. So the overall diffusion behavior in different structural forms (single crystalline, microcrystalline, nanocrystalline and amorphous) seems to be qualitatively similar to that in the extensively studied model system LiNbO₃ [32, 35, 36], although the diffusivity enhancements in the amorphous forms in the two systems differ quantitatively [31].

To sum up, the diffusion results obtained here on microcrystalline γ -LiAlO₂ are shown in Figure 8. The diffusion coefficients derived from the different methods are in agreement. The solid line is the linear fit of the Q_{avg} and SAE diffusion coefficients in the Arrhenius plot yielding an activation energy of 0.7 eV. The activation energy estimated from SLR NMR methods agrees with this result. It is known that activation energies from microscopic methods probing also short-range motion usually are smaller than those from macroscopic methods [29]. This effect which is mostly ascribed to correlated ionic motion was observed for both single crystalline [13] and microcrystalline (present work) γ -LiAlO₂.

4 Conclusion

Li ion diffusion in microcrystalline γ -LiAlO₂ was studied with several NMR methods and impedance spectroscopy. All our NMR results are in agreement with the NMR result from the literature for single crystals [13]. The activation energy estimated from NMR ($E_a = 0.7 \text{ eV}$) is also close to the activation energy from our impedance spectroscopy data (0.9 eV). When compared with the Li diffusivities of the amorphous and the nanocrystalline forms, those of the microcrystalline γ -LiAlO₂ are lower, as expected.

Acknowledgement: Financial support from the Deutsche Forschungsgemeinschaft (DFG) in the framework of the Research Unit FOR 1277 (molife) as well as GEENI (“Graduiertenkolleg Energiespeicher und Elektromobilität Niedersachsen”) is gratefully acknowledged.

References

1. E. J. Frazer and S. Phang, *J. Power Sources* **6** (1981) 307.
2. R. Boehmer, K. R. Jeffrey, and M. Vogel, *Prog. Nucl. Magn. Reson.* **50** (2007) 87.
3. J. Rahn, E. Hüger, L. Dörner, B. Ruprecht, P. Heitjans, and H. Schmidt, *Phys. Chem. Chem. Phys.* **14** (2012) 2427.
4. P. Heitjans and M. Wilkening, *MRS Bull.* **34** (2009) 915.
5. U. Bauer, A.-M. Welsch, H. Behrens, J. Rahn, H. Schmidt, and I. Horn, *J. Phys. Chem. B* **117** (2013) 15184.
6. S. Thinius, M. Islam, P. Heitjans, and T. Bredow, *J. Phys. Chem. C* **118** (2014) 2273.
7. H. Buschmann, J. Dölle, S. Berendts, A. Kuhn, P. Bottke, M. Wilkening, P. Heitjans, A. Senyshyn, H. Ehrenberg, A. Lotnyk, V. Duppel, L. Kienle, and J. Janeček, *Phys. Chem. Chem. Phys.* **13** (2011) 19378.
8. M. Wilkening and P. Heitjans, *J. Phys.: Condens. Mater.* **18** (2006) 9849.
9. M. A. K. L. Dissanayake, *Ionics* **10** (2004) 221.
10. S. Terada, I. Nagashima, K. Higaki, and Y. Ito, *J. Power Sources* **75** (1988) 223.
11. P. Waltereit, O. Brandt, and K. H. Ploog, *Appl. Phys. Lett.* **75** (1999) 2029.
12. J. Lin, Z. Wen, X. Xu, N. Li, and S. Song, *Fusion. Engin. Design* **85** (2010) 1162.
13. S. Idris, P. Heitjans, R. Uecker, and B. Roling, *J. Phys. Chem. C* **116** (2012) 14243.
14. H. Cao, B. Xia, Y. Zhang, and N. Xu, *Solid State Ionics* **176** (2005) 911.
15. J.-P. Jacobs, M. A. San Miguel, L. J. Alvarez, and P. B. Giral, *J. Nucl. Mater.* **232** (1996) 131.
16. F. Alessandrini, C. Alvani, S. Casadio, M. R. Mancini, and C. A. Nannetti, *J. Nucl. Mater.* **224** (1995) 236.
17. J. P. Jacobs, M. A. S. Miguel, L. J. Alvarez, and P. B. Giral, *J. Nucl. Mater.* **232** (1996) 131.
18. Q. Hu, L. Lei, X. Jiang, Z. C. Feng, M. Tang, and D. He, *Solid State Sci.* **37** (2014) 103.
19. S. Idris and P. Heitjans, *Phys. Rev. B* **74** (2006) 245120.
20. D. Wohlmuth, V. Epp, P. Bottke, B. Bitschnau, I. Letofsky-Papst, M. Kriechbaum, H. Amenitsch, F. Hofer, M. Wilkening, and I. Hanžú, *J. Mater. Chem. A* **2** (2014) 20295.
21. J. Rodriguez-Carvajal, *Abstracts of the Satellite Meeting on Powder Diffraction of the XV Congress of the IUCr, Toulouse, France* (1990) 127.
22. J. Jeener and P. Broekaert, *Phys. Rev.* **157** (1967) 232.
23. L. Lei, D. He, Y. Zou, W. Zhang, Z. Wang, M. Jiang, and M. Dub, *J. Solid State Chem.* **181** (2008) 1810.
24. D. Müller and W. Gessner, *Polyhedron* **2** (1983) 1195.
25. M. J. Duer, *Introduction to Solid-State NMR Spectroscopy*, Blackwell Publishing, Oxford (2004).
26. P. Pyykkö, *Z. Naturforsch.* **47a** (1992) 189.
27. H. Orth, H. Ackermann, and E. W. Otten, *Z. Phys. A* **273** (1975) 221.

28. D. Massiot, F. Fayon, M. Capron, I. King, S. Le Calve, B. Alonso, J. O. Durand, B. Bujoli, Z. H. Gan, and G. Hoatson, *Magn. Reson. Chem.* **40** (2002) 70.
29. P. Heitjans, A. Schirmer, and S. Indris, in: *Diffusion in Condensed Matter – Methods, Materials, Models*, P. Heitjans and J. Kärger (Eds.), Springer, Berlin (2005).
30. M. Wilkening and P. Heitjans, *Diff. Fundamentals* **6** (2007) 40.1.
31. J. Rahn, E. Witt, P. Heitjans, and H. Schmidt, *Z. Phys. Chem.* (2015), DOI [10.1515/zpch-2014-0658](https://doi.org/10.1515/zpch-2014-0658)
32. P. Heitjans, M. Masoud, A. Feldhoff, and M. Wilkening, *Faraday Discuss.* **134** (2007) 67.
33. A. Kuhn, E. Tobschall, and P. Heitjans, *Z. Phys. Chem.* **223** (2009) 1359.
34. M. Wilkening and P. Heitjans, *ChemPhysChem* **13** (2012) 53.
35. J. Rahn, E. Hüger, L. Dörrer, B. Ruprecht, P. Heitjans, and H. Schmidt, *Z. Phys. Chem.* **226** (2012) 439.
36. B. Ruprecht, J. Rahn, H. Schmidt, and P. Heitjans, *Z. Phys. Chem.* **226** (2012) 431.